BUTTERWORTH HEINEMANN

Polymer Vol. 36 No. 25, pp. 4787–4795, 1995

0032-3861/95/$10.00+0.00

Microstructural fracture processes accompanying growing cracks in tough rubber-modified polyamides

O. K. Muratoğlu*, A. S. Argon† and R. E. Cohen‡
Massachusetts Institute of Technology, Cambridge, MA 02139, USA

and M. Weinberg
E. I. du Pont de Nemours & Company, Central Research and Development Department, Experimental Station, Wilmington, DE 19898, USA
(Received 17 January 1995; revised 19 May 1995)

The process of massive cavitational deformation in an ethylene–propylene–diene grafted maleic-anhydride modified polyamide 66, initiated from cavitating rubber particles and associated with stable crack propagation in compact tension and Izod impact experiments, has been studied in the region ahead of the crack front by scanning electron microscopy. The very tough stable ductile tearing behaviour of the material was manifested by steady-state crack opening angles of 60° and large stress-whitened zones. The process zone ahead of the advancing crack comprised two regions with distinct morphologies: (a) within a radius of 30 μm in an 'intense' deformation zone in front of the crack, the cavities are elongated to large draw ratios ($\sim$ 10); and (b) in the remaining 'weak' zone cavities were found to be substantially equiaxed. The material with the elongated cavities of the crack front is parted by the propagating crack and immediately sheared by $\sim$ 60° and left lying parallel to the crack flank surfaces. The very tough behaviour of the material has been analysed by the well known mechanics of fracture of tough structural materials, and the calculated tearing moduli were found to be quite comparable with those of the toughest structural steels.

(Keywords: rubber-modified polyamide; crack growth; fracture mechanism)

INTRODUCTION

The processes of crack initiation and growth in fracture of moderately tough materials have been extensively studied and a number of mathematical models have been proposed (for an overview see Hutchinson[1]). The initiation stage is well understood and successful quantitative models have been developed for cases in which the material is only moderately tough so that the crack growth instability can be satisfactorily described by the so-called small-scale yielding approximations. Modelling the processes associated with a growing crack is far more complex. In very tough materials where crack growth is often stable in finite size parts, the crack advance conditions can best be viewed as a finite and relatively large crack opening angle. For such materials, extending the crack requires a continued albeit decreasing rate of increase of the crack driving force J. The toughness of the material is often described by a so-called tearing modulus T, defined as $(E/\sigma_0^2)\,(\mathrm{d}J/\mathrm{d}a)_{\mathrm{in}}$ where E and σ_0 are the Young's modulus and the plastic resistance in tension, respectively, and $(\mathrm{d}J/\mathrm{d}a)_{\mathrm{in}}$ is the initial rate of increase of the crack tip driving force J with crack length a to initiate crack advance (for succinct definitions of crack driving forces, particularly the so-called J integral, see Hutchinson[1]). A very useful and clear model of the complex mechanics of this process is described by Rice and Sorensen[2]. Rubber-modified polyamide blends (nylon 6 or 66) are very tough materials and furnish excellent examples for stable crack advance with very substantial crack opening angles[3].

The model material used in the present study is a rubber-toughened polyamide. The effect of various parameters in this toughening process such as that of particle size, rubber concentration, temperature and interparticle distance have been studied extensively[4–11]. Recently, Muratoğlu *et al.* proposed a mechanism of toughening of such semicrystalline polymers based on the lowering of the local plastic shear resistance in the interparticle ligament regions by the preferred orientation of the low slip resistance hydrogen-bonded slip planes of lamellae ((0 0 1) for polyamide 6 and (0 1 0) for polyamide 66) parallel to the rubber–matrix interface[12]. The reduction of the local flow stress prevents premature catastrophic failure and large local deformations are accommodated in the matrix before fracture occurs. Morphological studies in the stress-whitened zone of the

* Program in Polymer Science and Technology and Department of Material Science and Engineering
† Department of Mechanical Engineering. To whom correspondence should be addressed
‡ Department of Chemical Engineering

tough blends showed that the rubber particles cavitate and elongate to large draw ratios ($\sim$ 12) in the direction of the local principal stretch axis[13,14]. The evolution of the cavities and their spatial distribution have been examined by Muratoğlu *et al.* in considerable detail from the crack flanks into the interior region of an Izod impact tested tough polyamide 66 (PA66)/ethylene–propylene–diene rubber (EPDR) blend. Using the stretched-out cavities as built-in strain gauges, the local draw ratio and the orientation of the principal stretch axis were measured as a function of depth away from the crack flank[13].

EXPERIMENTAL

Sample preparation and characterization

A 28 mm Werner & Pfleiderer extruder was used to blend polyamide 66 with maleic anhydride functionalized ethylene–propylene-diene rubber (PA66/EPDR) at a rubber concentration of 20 wt%. The particle size was kept constant at around 0.32 μm by choosing the right maleic anhydride functionality level in the rubber components of the blend[13]. The resulting blends were pelletized and then moulded in a 6 oz, 150 ton Van Dorn injection moulding machine into flexural test bars (length = 127 mm, thickness = 3.2 mm) and 6.4 mm thick sheets. The Izod bars were cut from the middle part of the flexural bars. Notches were introduced into each Izod bar with a TMI Notching Cutter according to the specifications of ASTM D256.

The compact tension specimens were machined from the 6.4 mm thick injection moulded sheets in the form schematically shown in *Figure 1*. Two grooves on both sides and a chevron notch were machined in the specimens to prevent deviation of the crack plane from the plane of symmetry of the specimen, and to achieve reproducible initiation of crack growth. The side grooves were machined in the form of 0.5 mm deep, 90° V-notches. *Figure 2* summarizes the dimensions of the specimen which, as can be seen, was made longer than usual to achieve a good approximation to steady growth. Following the injection moulding, notching and machining processes, the samples were placed in air-tight bags and stored in a desiccator to prevent further absorption of water and to achieve uniformity in response of all specimens[15].

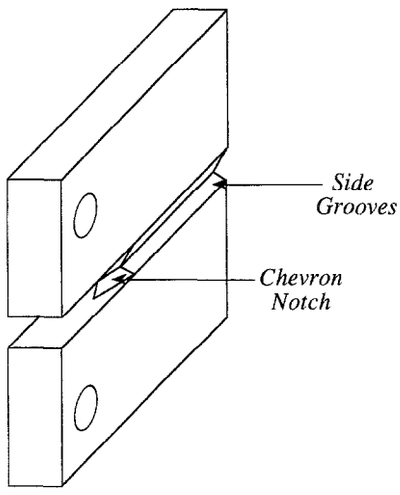

Figure 1 Sketch of the compact tension specimen with a chevron notch. Side grooves are machined in on both sides of the specimen to ensure planar crack propagation

Izod impact experiments

The Izod impact tests were carried out following ASTM D256 standards. The procedure to view the crack front morphology is schematically summarized in *Figure 3*. In the Izod impact test, a pendulum hits and breaks the specimen. However, since the material used for this study is of very high toughness, the fracture is incomplete. That is, as a result of the large rotations of the sample arms accompanying the large crack opening angles, the Izod bar bends and the pendulum swings by. As shown in *Figure 3*, the partially broken samples are taken out of

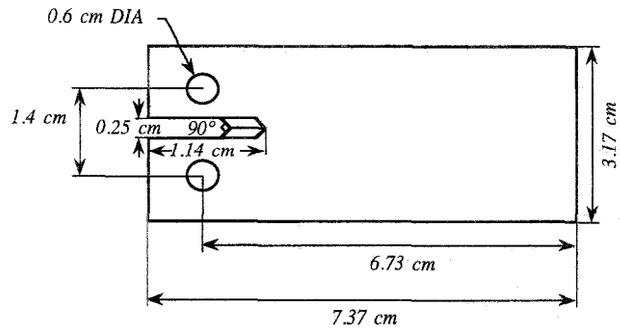

Figure 2 Dimensions of the compact tension specimen machined from the injection moulded sheets. The specimen is 6.4 mm thick and contains side grooves, each 0.5 mm deep

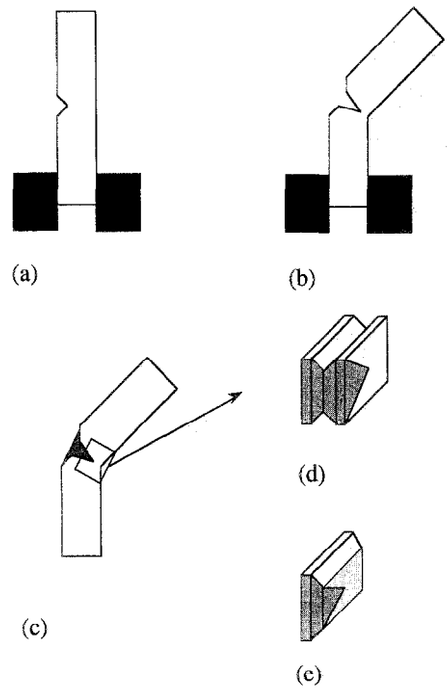

Figure 3 Fracture and preparation for microscopy of Izod impact specimens: (a) and (b) depict the Izod impact test where the specimen does not break and the pendulum swings by; (c) the opened crack is filled with epoxy; (d) a small section is cut from the crack front region and four notches are introduced around the cut piece; (e) a wedge is driven in to one of the four notches at liquid nitrogen temperature to expose the lightly shaded internal surface for microscopy

the Izod tester; the opened crack is filled with a low shrinkage, low viscosity epoxy (Epofix resin purchased from Struers); the specimen is left overnight to achieve complete cure of the epoxy filling; a small section of the specimen containing the crack tip is cut out; and four notches are introduced around the cut section as shown in *Figure 3d*. After 20 min soaking in liquid nitrogen, a wedge is driven through one of the notches to expose the lightly shaded area of *Figure 3e* for microscopy.

Compact tension experiments

The machined compact tension specimens were tested in an Instron 4200 universal testing machine at a crosshead speed of 500 mm min^{-1}. *Figure 4* schematically represents the procedure that was followed to propagate the crack in the specimen quasi-statically. The specimen was progressively torn apart in the Instron machine until a total pin to pin displacement of $\sim$ 20 mm was reached. A typical load–pin displacement curve is shown in *Figure 5*. The progressive decline of the tearing load is a result of the decreasing length of untorn specimen. Without removing the load, the opened crack was then framed from two sides by two strips of Scotch tape and filled with the low shrinkage, low viscosity epoxy (Epofix resin). The specimen was then held under load for 12 h to ensure total curing of the epoxy filling. Once the epoxy had hardened, the specimen was unloaded and a small section around the crack tip was cut (see *Figures 4c* and *d*). To examine the internal morphology of the cavities by scanning electron microscopy (SEM), four notches were introduced around the piece as shown in *Figure 4d* and a wedge was driven through one of the notches after the specimen was left in liquid nitrogen for > 20 min.

The exposed internal surfaces of both the compact tension and Izod bars were then coated with Au and the morphology of the cavities was examined in an Elektroscan environmental scanning electron microscope (ESEM). The microscope used a lanthanum hexaboride (LaB_6) filament and was operated at an accelerating voltage of 15 kV.

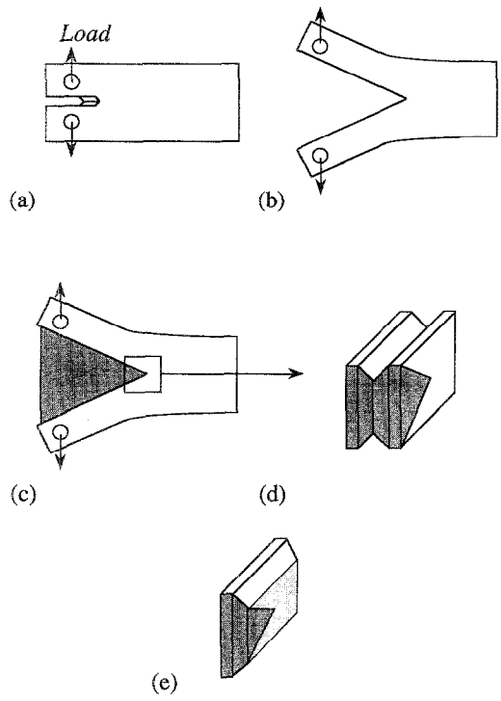

Figure 4 Testing of the compact tension specimen: (a) the specimen is pulled in an Instron machine at a crosshead speed of 500 mm min^{-1} to a normal displacement of $\sim$ 20 mm; (b), (c) the opened crack is filled with epoxy while the specimen is kept under load; (d) upon hardening of the epoxy the load is removed and the indicated square region is cut out of the specimen, notches are introduced on all four sides of the cut piece; and (f) a wedge is driven through one of the notches at liquid nitrogen temperature to expose the lightly shaded internal surface for microscopy

RESULTS AND DISCUSSION

Method of examination of deformation gradients around the crack

The model material used in the present study was a rubber-toughened polyamide 66 modified with 20 wt% rubber particles of 0.34 μm diameter (PA66/EPDR). Early studies have shown that under various stress states, the rubber particles cavitate[12,16,17] and the cavity elongates in the direction of the principal stretch axis **S** to large draw ratios[12–14,18]. Matrix ligaments can withstand such large stretches (draw ratios of $\sim$ 10) because the initially built-in local preferred orientation of the low slip resistance hydrogen-bonded planes parallel to the rubber–matrix interface facilitates large deformations by undergoing lamellar shear followed by textural alignment[12]. During elongation, the width of the cavities does not change significantly for reasons described in the earlier study[12]; hence the aspect ratio of the elongated cavities provides an estimate of the level of local draw ratio λ in the material. If the morphology of the cavities in a deformed material can be examined, the aspect ratio and direction of the major axis of the sausage shaped cavities on the micrographs can be used to determine the actual local draw ratio and direction of the principal stretch axis, respectively. The following two sections describe two methods used in this study to determine the morphology of the cavities around a propagating crack front which clearly reveal the variations of the local parameters (**S**, λ) around the crack tip for material

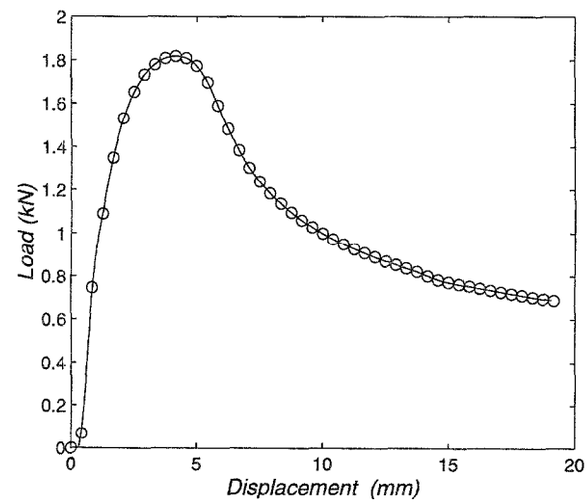

Figure 5 Load–pin displacement curve of the compact tension specimen tested at a crosshead speed of 500 mm min^{-1}, net specimen thickness is 5.4 mm

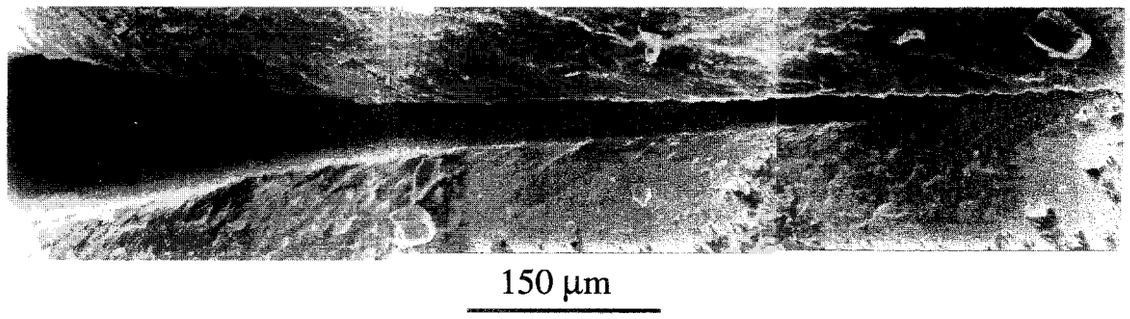

Figure 6 SEM micrograph of the stopped crack front in the Izod impact test, showing evidence of reverse deformation by touching of rebounding crack flanks

elements flowing towards the crack front, separating and being deposited along the crack flank.

Crack closure in Izod impact samples

The microscopy of the crack tip of Izod impact tested specimens showed that a substantial decrease of crack opening angle occurs due to the springback of the Izod bar after the pendulum swings by. The maximum crack opening angle during the Izod test is calculated to be around 60° based on the geometry of the pendulum swing and the angle where the pendulum loses contact with the specimen. After the test, the crack angle decreases to a residual opening of ~ 20° as measured from *Figure 6*. The reversal of the crack angle is not readily obvious from this micrograph. However, *Figure 7* showing the crack tip at higher magnification reveals the extensive buckling of the crack front as a result of the crack closure. The folding of the elongated cavities and the undulations in a surface layer of thickness 15–20 μm are clearly discernible on this micrograph. Therefore, the morphologies of the cavities are altered by the closure process and this method cannot be used in determining the crack tip morphologies in rubber-modified polyamides. The following section discusses the second method where the crack in a quasi-statically deformed compact tension specimen is filled with epoxy while it is held under load, preventing the springback of the sample. Hence no crack closure takes place and the cavity microstructure around the crack tip is substantially unaltered.

Crack tip microstructural alterations in compact tension specimens

The compact tension experiments were performed in an Instron machine and the final shape of the advanced crack was preserved by infiltrating the large crack opening with a low viscosity, low shrinkage epoxy as described above. As *Figure 4* summarizes, the morphology of the cavities around the crack front was examined in an SEM on a cryo-fractured surface containing the crack tip. *Figure 8* shows typical micrographs from various parts of the crack front. The smooth filling inside the crack is epoxy. Microscopically, the opening angle is measured to be ~ 60° which is consistent with the macroscopic crack opening angle (~ 60°) measured from the final opening of the crack while it was held under load in the Instron machine. Such large opening angles have been reported for rubber-modified polyamides by Huang[3] in *in situ* studies of crack propagation in rubber-toughened polyamide 66 in a field emission scanning electron microscope. The microscopic observations of Huang also revealed that the crack tip is blunted before growth is initiated. When stable crack growth conditions were reached, the profile of the tip resembled the schematic shapes shown in *Figure 9*. The top sketch is the side view of the crack front before initiation with a sharp tip. First, blunting occurs at the crack tip in the initial stages of deformation. When the critical crack opening displacement is reached the crack propagation initiates. Eventually steady-state growth will be reached and the flanks will curve towards the crack tip. The latter stage of the crack propagation evolution demonstrated by Huang, is in agreement with our light microscope examination of the epoxy-filled crack tip.

There is no indication of crack closure in epoxy-infiltrated compact tension specimens. The morphology at the crack tip recorded at high magnifications does not show any large-scale buckling of the cavities and folding of the fracture surface (see *Figures 8a–d*). Therefore, the morphology of the cavities is not altered; and this method can be used to determine the variations in the local draw ratios around the advancing crack front.

The uniform macroscopic stress whitening around the propagating crack defines the boundaries of the process zone, where the whitening is due to the cavitation of the rubber particles. However, on a microscopic scale, the morphology of the process zone varies significantly. There are two distinct morphologies as shown in *Figure 8b*, representing the area within a radius of 30 μm ahead

Figure 7 SEM micrograph of the stopped crack front in the Izod impact test, recorded from the side view as shown in *Figure 4*. Extensive folding of the flank surface layer and buckling of the elongated cavities are readily discernible

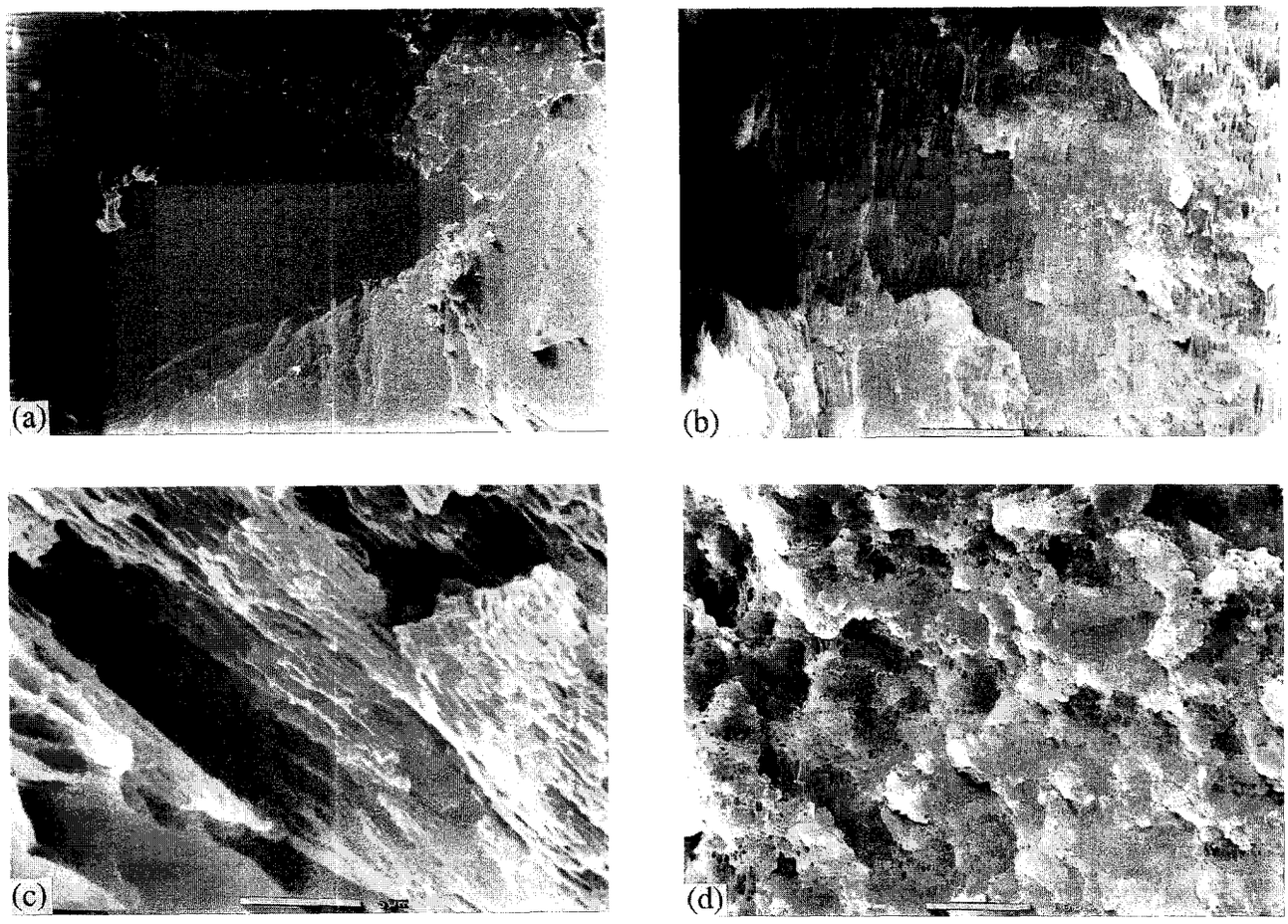

Figure 8 SEM micrographs showing the variations in the morphology of the cavities within the process zone. The location of each micrograph with respect to the crack is also indicated in the schematic of *Figure 10*: (a) the crack environment; (b) the crack tip region of 'intense' deformation; (c) below the crack flank; and (d) far field ahead of the crack front. *Figure 4* shows the method followed to expose the cavity morphology around the advancing crack tip

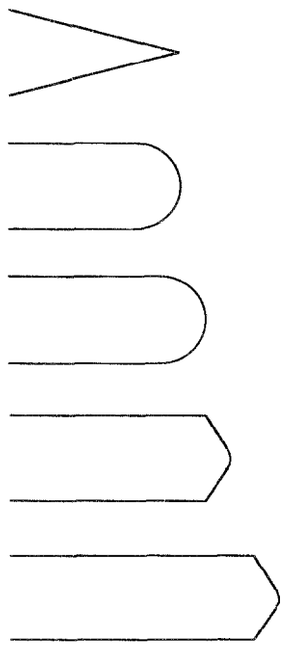

Figure 9 Profile of the advancing crack front in rubber-modified polyamide 66 proposed by Huang[3]

of the crack front, and *Figure 8d* records from the far field ahead of the crack front. The former region will be referred to as the 'intense' process zone, with the latter as the 'weak' process zone in the remainder of this communication. In the 'intense' process zone cavities are elongated to large draw ratios of around 10, whereas the 'weak' process zone consists of equiaxed, spherical cavities. As the crack propagates, the material immediately ahead of the crack front starts to come apart, probably when the matrix ligaments reach their ultimate draw ratio. The elongated cavities of this region then undergo a rotation of $\sim 60°$ about the crack front. Hence, the morphology of the cavities immediately beneath the fracture surface comprises a thin layer of elongated cavities aligned parallel to the crack flanks (see *Figure 8c*). *Figure 10* schematically represents the morphology of the cavities in the process zone. The lightly shaded region is where the cavitation is homogeneous with a spherical pore structure. The darkly shaded region in front of the crack tip is where the cavities are extended to large draw ratios. This region is then divided in two, and is left on the surface of the crack flanks as the crack propagates. The highly stretched cavities on and under the parting surfaces undergo a rotation of $\sim 60°$. As the micrograph of a flank region of *Figure 11* indicates, the thickness of the zone of elongated cavities that were rotated by a crack advance is about

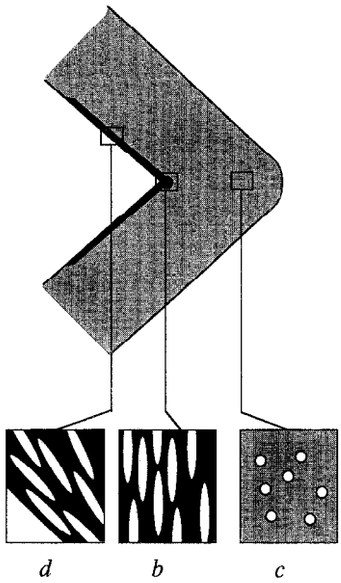

Figure 10 Schematic representation of the process zone around a crack propagating at steady state. The dark shaded area in the 'intense' process zone which is translated to the crack flank surface by the shear and rotation of the cavities upon parting of the material at the crack front. The magnified sketches of the cavity shapes shown in frames b,c,d, correspond to micrographs b,c,d in *Figure 8*

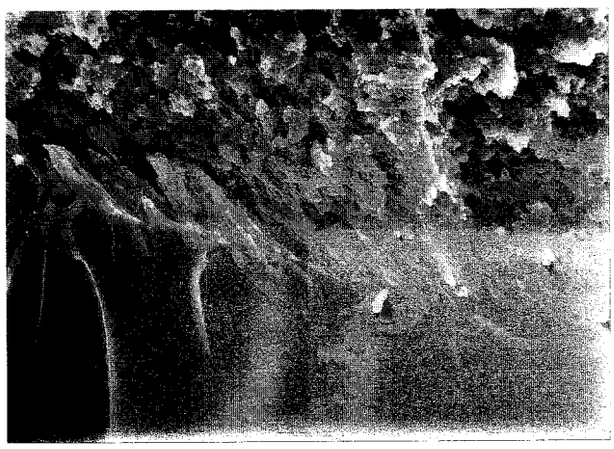

Figure 11 Morphology of the cavities above the upper crack flank. The thickness of the highly deformed layer on the flank surfaces with the distinct morphology of rotated and elongated cavities is $\sim 30\,\mu m$

$30\,\mu m$, which is very close to the radius of the 'intense' process zone, namely $30\,\mu m$, before it parts. Thus, the elongated cavities of the flank surface region originate from the 'intense' process zone and are simply rotated and translated to their final positions at the crack flanks, immediately behind the crack tip. The schematic of *Figure 12* summarizes the cavitated material flow with shear and rotation around the propagating crack front with a large opening angle. The flanks curve smoothly towards the crack front where they join in on the blunt tip. The principal axes of the cavities within the 'intense' process zone at the blunt tip are placed parallel to the flank surfaces as the rupturing crack tip material parts in two. Thus, the cavities beneath the freshly formed fracture surface suffer a substantial rigid body rotation, resulting from the shear of the parting material.

The evolution of the morphology around the propagating crack front could also be visualized alternatively as the relative flow of the rubber particles from right to left by an observer travelling with the blunted crack tip. As the particles approach the crack, they start to feel its intensifying stress field. Cavitation of the rubber and elongation of the surrounding matrix perpendicular to the crack plane intensifies as the particles get closer to the front. Upon division of the material flow in two and passage of the parts by the front, the cavities near the flanks rotate with the intense final shear of the parted material. Further away from the plane of the crack and the flanks, the rotation will be less severe due to the much lower concentration of shear strain in this region as is depicted in the schematic view of *Figure 12*. The sub-flank morphology of the cavities with the distribution of the level of cavitational strain and its principal stretch directions below the fracture surface have been described in detail elsewhere[13].

Two distinctive zones ahead of the advancing crack front and below the crack flank have also been observed by Sue and Yee[19] in polyamide/poly(phenylene oxide) (PA/PPO) blends. Their modifying phase (PPO) is a rigid polymer. Therefore, the samples exhibit smaller crack opening angles and the modifying rigid particles do not cavitate. Large deformations are accommodated by some elongation of the particles followed by their debonding at the interfaces and elongation of the surrounding cavities. Morphological analysis of the crack front showed that the process zone incorporated widespread cavitation but contained a central region of more intense shear in the cavitated zone. Below the crack flank, the authors observed a thin sheared layer near the fracture surface in the previously cavitated material. Similar morphological observations were made by the authors as reported in the present study. From the micrographs of Sue and Yee[19] showing the processed morphology, the angle between the flank and elongated cavities underneath the fracture surface can be estimated to be 60° which is much larger than that ($\sim 10°$, nearly parallel to the flank) encountered in this study. In fact, the rotation imposed by the advancing crack on the elongated cavities is $\sim 60°$ for both the PA/PPO (as measured from the micrographs of ref. 19) and the present PA66/EPDR blends. Yet, the crack opening angle in our blends is much larger than theirs. This is why the orientation of the elongated cavities below the flank surfaces is different.

Distribution of local deformation

To determine the local draw ratios, 25 micrographs were recorded from a thin strip ahead of the crack front. When connected together, they represent an area of $30\,\mu m \times 0.5\,mm$. The local draw ratios were estimated by measuring the aspect ratios of the cavities at various distances from the crack tip. *Figure 13* is a plot of the draw ratio as a function of distance away from the crack front. Within the 'intense' process zone the local draw ratio is constant at 10 but rapidly drops to 1 within a distance of $30\,\mu m$, beyond which it remains constant for the remainder of the process zone of roughly 1 cm length. *Figure 13* is similar to Figure 18 of our previous study[13]

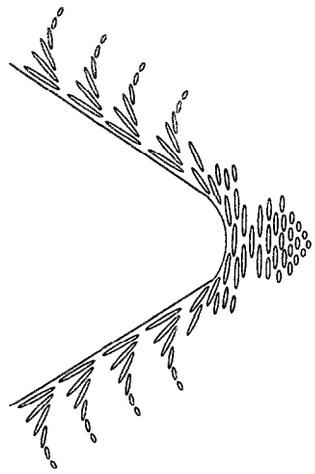

Figure 12 Schematic rendering of the travelling crack processing the morphology of the cavities in the material 'flowing-by' the propagating crack

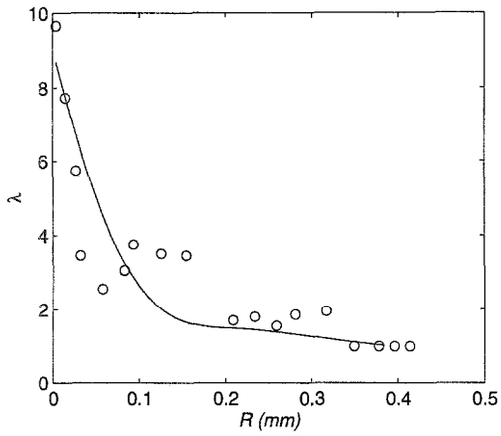

Figure 13 Distribution of the local draw ratios in the region ahead of the crack front in the plane of the crack

and Figure 13 of ref. 14 where, respectively, the variations of the local draw ratio and the length of the elongated cavities are plotted as a function of depth away from the crack flank. In the present study, the rate of deformation in the compact tension (CT) specimen was much lower in comparison with that of the Izod impact experiments of refs 13 and 14. Still, the thickness of the 'intense' process zone in all samples was $\sim 30\,\mu$m and it appears to be independent of the deformation rate. On the other hand, the maximum draw ratio observed in the CT specimens (low strain rate) is ~ 10 while that value was > 12 for Izod impact specimens (high strain rate). This could be due to high rate deformation induced adiabatic heating and temperature rise in the process zone that would in turn lower the flow stress of the material and allow it to deform to larger draw ratios.

Toughness of rubber-modified polyamide

The experiments reported above indicate that the rubber-modified polyamides are remarkably tough materials. Therefore, it is of interest to evaluate their behaviour in a quantitative framework to permit more meaningful comparison with other tough materials.

Materials which do not exhibit fracture instabilities in the usual laboratory experiments, such as the special compact tension specimen used in the present study, require special consideration to evaluate their toughness levels. It is customary to present the specific fracture work of such materials by means of the J integral, which characterizes the crack environment for the fracture process of materials undergoing large strain plasticity. In such tough materials the J integral will rise monotonically with crack extension until a steady-state value J_{ss} of the J integral is reached for the local process of separation. This type of behaviour, giving the required rise of J with increasing crack length, is known as a fracture resistance (R-curve) curve. Depending on the specimen or part geometry and the mode of loading, an eventual fracture instability is usually encountered before a steady-state J_{ss} is reached. In the present experiments with specimens of progressively increasing compliance, such instabilities were not reached. The characteristic load–pin displacement curve of *Figure 5* constitutes stable behaviour.

To obtain a measure of the material fracture toughness we nevertheless use the information provided in *Figure 5* to determine a crack driving force J, which we will interpret to be close to the steady-state J_{ss}.

The J integral, for a compact tension specimen of the type shown in *Figure 2* is[20]

$$J = \alpha\epsilon_0\sigma_0(1-\phi)c\,h_1\left(\frac{a}{b},n\right)\left(\frac{P}{P_0}\right)^n \qquad (1)$$

where

a = crack length measured from pin-line

b = distance from pin-line to free end of specimen

$c = b - a$

ϕ = volume fraction of rubber

$P_0 = 1.455\,\eta c\sigma_0(1-\phi)$

$\eta = [(2a/c)^2 + 2(2a/c) + 2]^{1/2} - (2a/c + 1)$

$\epsilon_e = \alpha\epsilon_0(\sigma_e/\sigma_0)^n$

where ϵ_e is the power-law fit, strain hardening expression, relating the stress σ_e and ϵ_e (equivalent quantities for three-dimensional behaviour), where $\alpha\epsilon_0$ and σ_0 are fitting constants. It is customary to consider σ_0 to be the yield stress of the material. The parameter $h_1(a/b,n)$, which is a tabulated function of a/b and n, is obtained from numerical solutions of the crack tip field[20]; P is the pin-load per unit specimen thickness t_s. In the present study the following magnitudes for the above quantities are appropriate for the geometric parameters:

$a = 5 \times 10^{-3}$ m

$b = 6.73 \times 10^{-2}$ m

$c = 6.23 \times 10^{-2}$ m

$t_s = 5.4 \times 10^{-3}$ m (taking account of side grooves)

$\eta = 0.371$

all determined from the CT specimen shape given in

Figure 2. For the material parameters, determined from data given by Lin and Argon[21], we have

$$\alpha\epsilon_0 = 3.95 \times 10^{-3}$$
$$\sigma_0 = 31.6\,\text{MPA}$$
$$n = 2.70$$
$$E_0 = 1300\,\text{MPa, Young's modulus}$$
$$\mu_0 = 500\,\text{MPa, shear modulus}$$
$$\phi_0 = 0.2 \text{ (given in the Experimental section; taken here as equal to the wt fraction)}$$

The numerical parameter $h_1(a/b, n) = 1.64$ was determined by interpolation and extrapolation of tabulated information of the CT specimen for the material parameters given above, for a plane stress problem.

From the peak load in *Figure 5* and t_s above we determine

$$P = 333\,\text{kN m}^{-1}$$

Moreover, the information above gives

$$P_0 = 870\,\text{kN m}^{-1}$$

With these values for the relevant parameters we determine the peak crack tip driving force J from equation (1), and interpret it as a good measure of the steady-state value J_{ss} as:

$$J_{ss} = 754\,\text{J m}^{-2} \tag{2}$$

The corresponding steady-state damage zone radius is[2]

$$R_{ss} = \lambda \frac{E}{\sigma_0^2} J_{ss} \approx 0.2\,\text{mm} \qquad (\lambda = 0.16)^2 \tag{3}$$

The comparison of the toughness of materials of this type is customarily facilitated by a so-called tearing modulus T defined as[2]:

$$T = \frac{E}{\sigma_0^2}\left(\frac{dJ}{da}\right)_{in} = \frac{\beta}{\alpha} \ln\left(\frac{J_{ss}}{J_{1c}}\right) \tag{4}$$

where $(dJ/da)_{in}$ is required initial rate of increase of the crack driving force with initiation of crack growth, and J_{ss}/J_{1c} is the ratio of the steady-state value to J_{1c}, the value to initiate crack growth. A model for the latter ratio has been given by Rice and Sorensen[2] as:

$$\frac{J_{ss}}{J_{1c}} = \frac{\alpha}{\lambda_e}\frac{\sigma_0}{E}\exp\left(\frac{E}{\sigma_0}\frac{1}{\beta}\theta^p\right) \tag{5}$$

where α, λ, β are theoretically determined constants, $e = 2.72$ is the basis of the natural logarithm, and θ^p is the steady-state plastic crack opening angle for the propagating crack. Rice and Sorensen[2] recommended the following magnitudes, based on crack tip numerical models,

$$\alpha = 0.50$$
$$\lambda = 0.160$$
$$\beta = 4(2-\nu)/\sqrt{3} = 3.9 \qquad (\nu = 0.3)$$

In the present experiments of fracture of the CT specimens, a steady-state total crack opening angle of 60° was determined under load. To determine the plastic crack opening angle we need to determine the elastic springback. A good measure of this can be readily obtained from the load–displacement curve of *Figure 5* by noting the pin displacement rate based on the initial slope of the curve and calculating the elastic pin displacement for the peak load. This for an initial crack length $a = 5\,\text{mm}$ gives an elastic rebound angle $\theta^e = 0.231\,\text{rad}$, which gives $\theta^p = 0.819\,\text{rad}$. Thus, we obtain from equations (5) and (4)

$$\frac{J_{ss}}{J_{1c}} = 158 \tag{6}$$

$$T = 39.5 \tag{7}$$

respectively. It is worth noting that in the evaluation of equation (5), σ_0/E appears as a ratio. Thus, the fact that the crack tip zone material is cavitated has no specific effect on the answer in equation (5), since the cavitation should affect σ_0 and E in the same way and the net effect should cancel. Therefore, we have used σ_0/E for the intrinsic polyamide.

Moreover, from equations (2) and (6) we obtain a value for the initial crack driving force J_{1c} to start crack growth as:

$$J_{1c} = 4.77\,\text{J m}^{-2} \tag{8}$$

Considering the possible substantial errors that can be made in the evaluation of equation (5) due to the uncertainty of the numerical constants, we consider this value as a low estimate.

Comparison with other tough materials

We note that the analysis of the toughness of the

Table 1 Crack growth parameters for specific pressure vessel steels compared with EPDR reinforced polyamide 66 (steel parameters based on data of Clark *et al.*[22], arranged by Rice and Sorensen[2])

Material	δ_{1c} (mm)	θ^p (rad)	σ_0/E	J_{ss}/J_{1c}	T_{init}
A533B (1 h 670°C, 36 h 620°C)	0.19	0.74	0.0024	8×10^{30}	555
A533B (4 h 650°C)	0.18	0.20	0.0028	2×10^5	94.5
HY-80 (5 h 650°C)	0.125 (average)	0.39 (average)	0.0035	5×10^9	174
HY-80 (20% prestrain)	0.045	0.12	0.0046	3.6	10.0
HY-130 (2 h 610°C)	0.06	0.13	0.0045	7.1	15.3
Weld deposit L (HY-80 MMA 4-pass)	0.03	0.02 (base material)	0.0035	0.02	[b]
Weld deposit N (HY-100 MMA 4-pass)	0.03	0.06 (base material)	0.0037	0.02	[b]
PA66/EPDR blend	[a]	0.82	0.0240	158	39.5

[a] Available information is too unreliable to determine initial critical opening displacement
[b] Spontaneous fracture

rubber-modified polyamide, given in the section above, is quite approximate since the crack tip material in the damage zone undergoes very substantial cavitation and develops very significant plastic anisotropies arising from the alignment of the stretched-out cavities. How these important effects modify the crack tip field and the model of Rice and Sorensen which we have used as a guide is unknown, and must be determined from a more specific numerical analysis which is planned. The great attraction of the rubber-modified polyamide with its quasi-regularly cavitating microstructure is that it can serve as an ideal model material to develop a quantitive understanding of the mechanics of fracturing and tearing of very tough materials, which has not been possible with the more irregular microstructures of tough structural alloys.

Here a comparison of the rubber-modified polyamides with tough structural steels is also enlightening. For this purpose we reproduce a comparative table assembled by Rice and Sorensen[2] of the performance of some of the toughest structural steels (see *Table 1*). We note that with a steady-state plastic crack opening angle of $\theta^p = 0.819$ rad, the rubber-modified polyamides lie above the best structural steels on a relative comparison. Admittedly, some of these steels have larger J_{ss}/J_{1c} ratios and much higher tearing moduli than rubber-modified polyamides. This is a direct result of their substantially smaller σ_0/E ratios which tend to amplify the tearing modulus. Even on this basis, however, the rubber-modified polyamides have relative behaviour commensurate with some of the best structural steels. In fact, comparison of the tearing modulus of the structural steels with that of the rubber-modified polyamides on a per unit mass basis (specific tearing moduli) would further emphasize the importance of these structural polymers.

CONCLUSIONS

To study the interaction of a growing crack with the cavitating microstructure of the very tough rubber-modified polyamides, Izod impact experiments and fracture of compact tension specimens were carried out. The former resulted in the forced closure of the crack due to the dynamic springback of the specimen after the pendulum swung by, therefore significantly altering the morphology of cavities by widespread buckling of ligaments. On the other hand, the compact tension specimens were deformed under stable crack growth conditions, with steady-state crack opening angles of 60°. The tearing process was studied in detail by 'freezing' the crack in its open condition by infiltrating the specimen with epoxy while it was held under load. SEM examinations of the propagating crack revealed the evolution of the morphology of the cavities in and around the crack front: in the far field the rubber particles cavitate forming spherical voids; near the crack front these elongated to draw ratios of ~ 10; past the crack front and below the crack flank, the elongated cavities are rotated by shear by $\sim 60°$ and become aligned parallel to the crack flank. Two distinct regions within the process zone can be distinguished: (i) an 'intense' process zone with elongated cavities and (ii) a 'weak' process zone with spherical cavities. The former is translated with large shears and rotations to the flank region upon the separation of the material at the crack tip as it advances.

The 'intense' and 'weak' process zones were observed only in tough blends of rubber-modified polyamides. The brittle blends are not endowed with the local preferred orientations of low resistance slip planes parallel to the rubber–matrix interface[12]; hence elongation of the cavities and crack tip blunting does not occur, leading to brittle failure.

The toughness of the rubber-modified polyamides was evaluated by the well known mechanics of fracture of very tough materials. The plastic crack opening angles and tearing moduli were found to compare very favourably with those of some of the toughest structural alloys on a relative basis.

ACKNOWLEDGEMENTS

Early stages of this research were supported by NSF/MRL through the Center for Materials Science and Engineering at MIT under DMR-90-22933 and by a DuPont Company Graduate Fellowship for OKM, for which we are grateful to Dr D. Huang of that company.

REFERENCES

1 Hutchinson, J. W. 'Non Linear Fracture Mechanics', The Technical University of Denmark, 1979
2 Rice, J. R. and Sorensen, E. P. *J. Mech. Phys. Solids* 1978, **26**, 163
3 Huang, D. D. 'Deformation Yield and Fracture of Polymers: 8th International Conference', Plastics and Rubber Institute, London, 1991
4 Hobbs, S. Y., Bopp, R. C. and Watkins, V. H. *Polym. Eng. Sci.* 1983, **23**, 380
5 Wu, S. *J. Appl. Polym. Sci.* 1988, **35**, 549
6 Borggreve, R. J. M. and Gaymans, R. J. *Polymer* 1989, **30**, 63
7 Oshinski, A. J., Keskkula, H. and Paul, D. R. *Polymer* 1992, **33**, 267
8 Majumdar, B., Keskkula, H. and Paul, D. R. *Polymer* 1994, **35**, 1399
9 Dijkstra, K., ter Laak, J. and Gaymans, R. J. *Polymer* 1994, **35**, 332
10 Borggreve, R. J. M., Gaymans, R. J., Schuijer, J. and Ingen-Housz, J. F. *Polymer* 1987, **28**, 1489
11 Wu, S. *Polymer* 1985, **26**, 1855
12 Muratoğlu, O. K., Argon, A. S., Cohen, R. E. and Weinberg, M. *Polymer* 1995, **36**, 921
13 Muratoğlu, O. K., Argon, A. S., Cohen, R. E. and Weinberg, M. *Polymer* 1995, **36**, 4771
14 Speroni, F., Castoldi, E., Fabbri, C. and Casiraghi, F. *J. Mater. Sci.* 1989, **24**, 2165
15 Lin, L. and Argon, A. S. *Macromolecules* 1992, **25**, 4011
16 Bucknall, C. B., Heather, P. S. and Lazzeri, A. *J. Mater. Sci* 1989, **16**, 225
17 Ramsteiner, F. and Heckmann, W. *Polymer* 1985, **26**, 199
18 Fukui, T., Kikuchi, Y. and Inoue, T. *Polymer* 1991, **32**, 2367
19 Sue, H. J. and Yee, A. F. *J. Mater. Sci.* 1989, **24**, 1447
20 Kumar, V., German, M. D. and Shih, C. F. 'An Engineering Approach for Elastic–Plastic Fracture Analysis,' (NP-1931 Research Project 1237-1), Electric Power Research Institute, Palo Alto, CA, 1981
21 Lin, L. and Argon, A. S. *Macromolecules* 1994, **27**, 6903
22 Clark, G. A., El Soudani, S. M., Ferguson, W. G., Smith, R. F. and Knott, J. W. 'Ductile Crack Extension in Pressure Vessel Steels', Institution of Mechanic Engineers, London, 1978